High-Pressure, High-Temperature Single-Crystal Growth, Ab initio Electronic Structure Calculations, and Equation of State of ε-Fe_3N_{1+x}

Rainer Niewa,*[,†] Dieter Rau,[†] Aron Wosylus,[‡] Katrin Meier,[‡] Michael Hanfland,[§] Michael Wessel,[||] Richard Dronskowski,[||] Dmytro A. Dzivenko,[⊥] Ralf Riedel,[⊥] and Ulrich Schwarz[‡]

Department Chemie, Technische Universität München, Lichtenbergstrasse 4, 85747 Garching, Germany, Max-Planck-Institut für Chemische Physik fester Stoffe, Nöthnitzer Strasse 40, 01187 Dresden, Germany, European Synchrotron Radiation Facility, 38043 Grenoble, France, Institute of Inorganic Chemisty, RWTH Aachen University, Landoltweg 1, 52056 Aachen, Germany, and Fachbereich Material- and Geowissenschaften, Fachgebiet Disperse Feststoffe, Technische Universität Darmstadt, Petersenstrasse 23, 64287 Darmstadt, Germany

Received October 7, 2008. Revised Manuscript Received November 25, 2008

The high-pressure behavior of the hard material ε-Fe_3N_{1+x} was studied up to 33 GPa with in situ X-ray diffraction experiments using diamond anvil cells in combination with synchrotron radiation as well as by ex situ high-temperature, high-pressure treatment at 1600(200) K in a two-stage multianvil device with a Walker-type module. Evaluation of the pressure−volume data up to 10 GPa by fitting a Murnaghan-type equation reveals a bulk modulus of $B_0 = 172(4)$ GPa ($B' = 5.7$, fixed). The calculated bulk modulus (220 GPa) on the basis of density-functional theory (GGA-PAW-PBE) is in satisfying agreement with the experimental one. Single crystals of ε-Fe_3N_{1+x} as obtained by ex situ high-temperature, high-pressure experiments reveal in X-ray diffraction data refinements a structural model of iron atoms in the motif of a hexagonal close packing with occupation of octahedral voids by nitrogen atoms exhibiting long-range order. The preferred structural model is described in space group $P312$ ($a = 4.7241(2)$ Å, $c = 4.3862(2)$ Å, $V = 84.773(6)$ Å^3, $Z = 2$, $R(F) = 0.0339$, $wR(F^2) = 0.0556$) and compared to a second model in $P6_322$. This choice of structural description is corroborated by the results of density-functional calculations. These yield a total energy at 0 K, which is 5 kJ/mol lower for the model in space group $P312$ compared to the second best alternative arrangement. Using micro- and nanoindentation techniques, a Vickers hardness of $H_V = 7.4(10)$ GPa, a nanoindentation hardness of $H = 10.1(8)$ GPa, as well as a reduced elastic modulus in the amount of $E_r = 178(11)$ GPa were measured for ε-Fe_3N_{1+x} single crystals.

Introduction

The chemistry of nitrides was significantly expanded in the last two decades as a result of instrumental developments and, most important, new synthesis methods leading to numerous prospective applications in a number of fields related to material-dependent science and engineering. An important parameter in the preparation of this class of compounds is pressure, because typically the reactivity of nitrogen and the stability of nitrides is considerably increased by application of high pressures. In materials science, nitrides are important for hard covers and bulk ceramics, e.g., for iron hardening and for the preparation of Si_3N_4 and BN. Research on minerals and meteors, respectively, normally deals with oxides and metals in experimental studies and theoretical models. Although thermodynamically not favored in oxygen containing atmospheres, nitrides are rare but present in earth's crust mostly originating from meteorites. Particularly, iron nitrides were found in nature because of formation of Siderazote (Silvestrite, Fe_5N_2 = phase from the ε-Fe_3N homogeneity range) in the proximity of active volcanoes, e.g., the Mount Etna and the Vesuvius,[1,2] and observation of Roaldit (γ'-Fe_4N) in meteroidic material.[3]

Because of the benefit in surface hardening to improve tribological properties, fatigue endurance, and corrosion resistance, as well as the potential as magnetic recording materials, the binary phase diagram Fe−N has been intensely studied for more than 50 years.[4,5] Already, Despretz[6] and Berthollet and Thénard[7] realized the useful refractory properties in the very first reports on binary iron nitrides. Nowadays, surface hardening by nitriding or carbonitriding of steel- and iron-based alloy workpieces is a well-known technology; however, many details about the involved iron-nitride phases

* To whom correspondence should be addressed. Tel.: 49 (0) 89-289-13111. Fax: 49 (0) 89-289-13762. E-mail: rainer.niewa@mytum.de.
† Technische Universität München.
‡ Max-Planck-Institut für Chemische Physik fester Stoffe.
§ European Synchrotron Radiation Facility.
|| RWTH Aachen University.
⊥ Technische Universität Darmstadt.

(1) Anthony, J.; Bideaux, R.; Bladh, K.; Nichols M. *Handbook of Mineralogy: Halides, Hydroxides, Oxides*; Mineral Data Publishing: Tuscon, AZ, 1997; Vol. 3.
(2) Silvestri, O. *Poggendorfs Ann. Phys. Chem.* **1867**, *157*, 165.
(3) Buchwald, V. F.; Nielsen, H. P. *Lunar Planet. Sci.* **1981**, *12*, 112.
(4) Frey, A. *Stahl Eisen* **1923**, *43*, 12.
(5) Andriamandroso, D.; Fefilatiev, L.; Demazeau, G.; Fournès, L.; Pouchard, M. *Mater. Res. Bull.* **1984**, *19*, 1187.
(6) Despretz, C. *Ann. Chim. Phys.* **1829**, *42*, 122.
(7) Berthollet, C. L.; Thénard, L. J. *Traité Chim.* **1834**, *i*, 434.

10.1021/cm802721k CCC: $40.75
Published on Web 12/22/2008

are still vague. This is partly due to the fact that all investigations were exclusively carried out on microcrystalline powders, microcrystalline layers produced under iron hardening conditions, or on thin films.

We present the first preparation of single crystals of a binary iron nitride obtained in a pressure-induced crystal growth, specifically Fe_3N_{1+x} from the so-called ε-Fe_3N type homogeneity range. A similar quality of single crystals with different composition started from γ′-Fe_4N and was recently summarized in a conference proceeding.[8] Density functional theory based methods of electronic-structure calculations[9,10] have been used, almost a decade ago, for the analysis of the entire 3*d* mononitrides and the five known nitrides of iron. The calculated ground-state properties were in good agreement with the available experimental data, and the importance of antibonding Fe−N states in the highest occupied bands close to the Fermi energy has been highlighted.

Experimental Section

Precursor Preparation and Characterization. Pure microcrystalline ε-Fe_3N_{1+x} was prepared by a reaction of iron powder (99.9%, Johnson Matthey/Alfa) in flowing NH_3 (99.98% NH_3, 20 sccm) at 520 °C (sccm = gas volume flow in cm^3 under standard conditions, 1.013 bar, per minute).

Chemical analyses on O and N were performed using the carrier gas hot-extraction technique on a LECO analyzer TCH-600. All values are averages of at least three independent measurements. Chemical analysis of the starting material results in a composition of $Fe_3N_{1.05\pm3}O_{0.017\pm1}$ (w(O) = 0.148 ± 0.007%, w(N) = 7.96 ± 0.30%). Hydrogen has been below the detection limit in all samples so far, with a typical lower bound of w(H) = 0.008%.

X-ray powder diffraction was carried out using an Imaging Plate Guinier Camera (HUBER diffraction, $CuK\alpha_1$ and $CoK\alpha_1$ radiation, 6 × 15 min scans, 8 ° ≤ 2θ ≤ 100 °).

Ex situ High-Pressure Crystal Growth and Characterization. High-pressure conditions were realized with a hydraulic uniaxial press. Force redistribution in order to achieve quasi-hydrostatic conditions was accomplished by a Walker-type module (two-stage assembly with a central octahedral pressure chamber)[11−14] and MgO/Cr_2O_3 octahedra with an edge length of 14 mm. Elevated temperatures were realized by resistive heating of graphite tubes containing the sample crucible. Pressure and temperature calibration had been performed prior to the experiments by analyzing the resistance changes of bismuth and lead[15] and measurements of set-ups equipped with W−W/Re thermocouples, respectively. The crucibles girdling the samples are made from hexagonal boron nitride. X-ray powder diffraction data do not give evidence for a chemical reaction of the container with the sample. Thus, separation of reaction products and crucible material can be achieved easily.

A typical high-pressure synthesis of bulk single-crystalline material requires pressure increase for 5 h to 15(2) GPa, holding at the maximal pressure for typically 5 h followed by decompression within 15 h. At the maximum pressure samples were heated at 1600(200) K for 5 min. Heated samples are quenched to ambient temperature by disconnecting the heating current before pressure release. Products were grayish-black compact cylindrical ingots with conchoidal fracture typical for macroscopic crystalline material. Larger crystalline particles exhibit a grayish-black metallic luster.

All isolated larger fragments showed discrete spots in X-ray single-crystal diffraction experiments; however, the largest pieces exhibiting a clear splitting of reflections at higher diffraction angles. Thus, a small irregular shaped single-crystal with about 17 μm edge lengths was used for structure analysis. Data collection was performed by means of a Rigaku R-axis spider diffractometer equipped with a rotating anode (Ag $K\alpha$ radiation) and an imaging plate detector.

In situ Diffraction Experiments at High Pressures. The iron nitride starting material ε-Fe_3N_{1+x} was ground into a fine powder and placed in steel gaskets using either a 4:1 methanol:ethanol mixture or argon as a pressure transmitting medium. High pressures were generated by diamond anvil cells and determined by the ruby luminescence method.[16,17] X-ray powder diffraction experiments were carried out at the undulator beamline ID09A of the ESRF, Grenoble. During the exposures, samples were oscillated by ±3° in order to enhance powder statistics. Typical exposure times were 2−5 s. The diffraction patterns were collected by means of an imaging plate detector which is positioned at a distance of approximately 450 mm from the sample. For calibration of wavelength (41.3 pm) and detector distance we used a silicon standard sample. Integration of the two-dimensional intensity data was performed using the pattern integration software image integrator.[18] Peak positions and lattice parameters were refined using the computer program WinCSD.[19]

Microhardness and Nanoindentation. Indentation measurements were performed on a mirror polished surface of ε-Fe_3N_{1+x} crystals. Vickers microhardness (H_V) was measured using a LECO M-400 G2 hardness tester. At least five indentations were made for each applied load from 5 g to 0.5 kg (from 0.049 to 4.9 N). Only two indentations were made at 1 kg load (9.8 N) because of limited sample surface. The loading time was fixed to 15 s. The lengths of impression diagonals were measured optically for high loads and by using a calibrated scanning electron microscope (Philips XL30 FEG) for low loads.

Nanoindentation experiments were performed on a Fischerscope H100 system (Fischer GmbH) equipped with a Vickers diamond indenter. Indentations were made for two maximum loads of 50 and 100 mN in 40 and 60 steps, respectively. At each step, the load was held for 1 s. The tip-shape function was calibrated using a standard BK7-glass supplied by Fischer GmbH. In order to derive the nanoindentation hardness (H) and the reduced elastic modulus (E_r) of ε-Fe_3N_{1+x}, the obtained load-displacement data were analytically processed by the method proposed by Oliver and Pharr.[20]

Electronical Structure Calculations. The ab initio calculations are based on the plane wave/pseudopotential strategy using the computer program VASP (Vienna Ab initio Simulation Package) [21,22] employing the generalized gradient approximation (GGA) of the

(8) Niewa, R.; Rau, D.; Wosylus, A.; Meier, K.; Wessel, M.; Dronskowski, R.; Schwarz, U. *J. Alloys. Compd*, in press.
(9) Eck, B.; Dronskowski, R.; Takahashi, M.; Kikkawa, S. *J. Mater. Chem.* **1999**, *9*, 1527–1537.
(10) Kroll, P.; Eck, B.; Dronskowski, R. *Adv. Mater.* **2000**, *4*, 12.
(11) Walker, D.; Carpenter, M. A.; Hitch, C. *Am. Mineral.* **1990**, *75*, 1020.
(12) Walker, D. *Am. Mineral.* **1991**, *76*, 1092.
(13) Walter, M. J.; Thibault, Y.; Wei, K.; Luth, R. W. *Can. J. Phys.* **1995**, *73*, 273.
(14) Rubie, D. C. *Phase Transitions* **1999**, *68*, 431.
(15) Young, D. A. *Phase Diagram of the Elements*; University of California Press: Berkeley, CA, 1991.
(16) Piermarini, G. J.; Block, S.; Barnett, J. D.; Forman, R. A. *J. Appl. Phys.* **1975**, *46*, 2774.
(17) Mao, H. K.; Bell, P. M.; Shaner, J. W.; Steinberg, D. J. *J. Appl. Phys.* **1978**, *49*, 3276.
(18) Akselrud, L. Image Integrator, version 1.2; Max-Planck-Institut für Chemische Physik fester Stoffe, Dresden, Germany, 2005.
(19) Akselrud, L. G.; Zavalii, P. Y.; Grin, Yu. N.; Pecharsky, V. K.; Baumgartner, B.; Woelfel, E. *Mater. Sci. Forum* **1993**, *335*, 133–136.
(20) Oliver, W. C.; Pharr, G. M. *J. Mater. Res.* **1992**, *7*, 1564.
(21) (a) Kresse, G.; Hafner, J. *Phys. Rev. B* **1993**, *47*, 558. (b) Kresse, G.; Hafner, J. *Phys. Rev. B* **1994**, *49*, 14251.

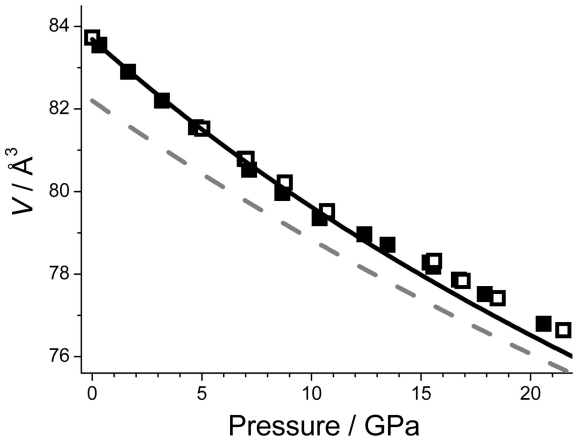

Figure 1. Pressure−volume data of ε-Fe_3N. The solid line shows the result of a least-squares fit of a Murnaghan-type equation of state to the experimental data up to 10 GPa. Open and filled symbols represent independent measurements. The gray dashed curve corresponds to the results of the density-functional calculations.

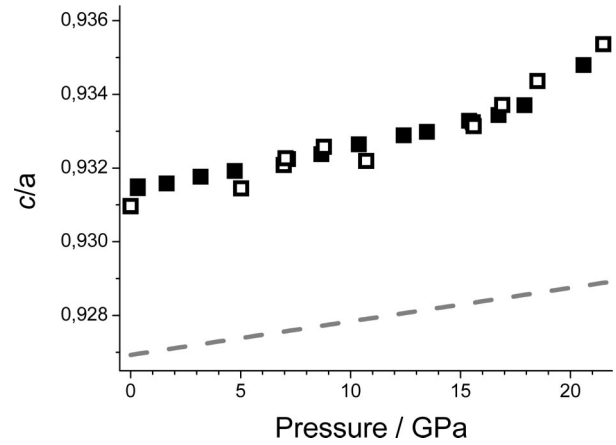

Figure 2. *c*/*a* ratio of the hexagonal unit-cell parameters of ε-Fe_3N as a function of pressure. Open and filled symbols represent independent measurements. The gray dashed curve represents the results of the density-functional calculations.

PBE type and the projected-augmented wave (PAW) method. A cutoff energy of 500 eV and a dense net of *k*-points was chosen to find the optimum structure lying lowest in energy. Thus, the unit cells were allowed to change in volume and shape, and all atomic positions were allowed to relax. Because of the small energy differences, the convergence criterion of the electronic structure calculation was set to 0.01 meV. This method has been successfully used for other ternary iron nitrides[23,24] prior to their synthesis. After finding the cell lowest in energy for each structure and composition, the volume was changed around the equilibrium volume and bulk modules were obtained by fitting Murnaghan-type equations of state to the calculated energies.

Results and Discussion

In situ X-ray diffraction experiments with synchrotron radiation performed on as-prepared single phase ε-Fe_3N_{1+x} with analytical composition $Fe_3N_{1.05\pm3}O_{0.017\pm1}$ in a diamond anvil cell lead to the volume−pressure dependence as presented in Figure 1. The data result from two measurements, one with larger pressure increments up to a maximum pressure of 33 GPa. The data give no evidence for a structural phase transition. A least-squares fit of a Murnaghan-type equation[25] of state to the experimental volume data is limited to a pressure of 10 GPa because the solidification of the pressure medium at higher pressures clearly shows in discontinuous changes that are attributed to shear forces and/or strain effects. The analysis yields a bulk modulus of B_0 = 172(4) GPa (B' = 5.7, fixed). Because B_0 and B' are strongly correlated in the refinement, we prefer these numbers over those obtained with free refinement of B' (B_0 = 177(8) GPa, B' = 5(2)); however, the resulting pressure−volume data calculated from both parameter sets (Figure 1) are virtually identical. A previous study of the compressibility with a similar technique produced B_0 = 168(10) GPa (B' = 5.7(1.5)).[26] Although the sample used in this older study designated as ε-$Fe_3N_{1.3}$ contained significant amounts of γ'-Fe_4N, making the unit-cell refinements as well as the composition assignment unreliable, the results are identical within experimental error. The zero-pressure volume as determined by ex situ X-ray powder diffraction with LaB_6 as an internal standard V_0 = 83.73(7) Å^3 is compatible with the reported value for the unit-cell volume of V = 84.47 Å^3 for a similar composition of $Fe_3N_{1.10}$.[27] For comparison, the bulk modulus of hexagonal high-pressure ε-Fe was determined to B_0 = 165(4) GPa (B' = 5.33(9), V_0 = 6.73(1) cm^3/mol) for pressures up to 300 GPa.[28]

Figure 2 shows the *c*/*a* ratio of the hexagonal unit cell as a function of pressure. As was observed earlier[26] the *c*/*a* ratio deviates toward lower values as compared to the hypothetical value for a hexagonal close packing of iron (0.943 = 1.633/$\sqrt{3}$) at ambient pressure. Upon pressure increase, the *c*/*a* ratio increases toward the ideal value. A possible change of slope of *c*/*a* around 15 GPa will be subject of further studies. The hexagonal high-pressure form of elemental iron (ε-Fe) reveals a deviation from the ideal value (*c*/*a* = 1.603), but the ratio decreases upon compression.[28] As shown in Figure 2 the ratio obtained from quantum theoretical computations is in excellent agreement with the experimental data. Nitrogen uptake apparently strengthens the crystallographic *c*-direction considerably more than the *a*-plane compared to pure iron ε-Fe.

Treatment of ε-$Fe_3N_{1.05\pm3}O_{0.017\pm1}$ in a multianvil press at p = 15(2) GPa and T = 1600(200) K for a duration of about 5 min reproducibly converts the microcrystalline powder into a compact well-crystallized material. This is the first report on a preparation of single crystals of a pure binary iron nitride. The unit-cell determination by powder X-ray diffraction (hexagonal, a = 4.7241 Å, c = 4.3862 Å compared to a = 4.7160 Å, c = 4.3859 Å for ε-$Fe_3N_{1.10}$[27]) indicates no significant change of composition during the high-

(22) (a) Kresse, G. Furthm̈; uller, J. *Comput. Mater. Sci.* **1996**, *6*, 15. (b) Kresse, G. Furthm̈; uller, J. *Phys. Rev. B* **1996**, *55*, 11169.
(23) von Appen, J.; Dronskowski, R. *Angew. Chem.* **2005**, *117*, 1230.
(24) Houben, A.; Müller, P.; von Appen, J.; Lueken, H.; Niewa, R.; Dronskowski, R. *Angew. Chem.* **2005**, *117*, 7379.
(25) Murnaghan, F. D. *Proc. Natl. Acad. Sci. U.S.A.* **1944**, *30*, 244.
(26) Adler, J. F.; Williams, Q. J. *Geophys. Res.* **2005**, *110*, B01203.
(27) Leineweber, A.; Jacobs, H.; Hüning, F.; Lueken, H.; Kockelmann, W. *J. Alloys Compd.* **2001**, *316*, 21.
(28) Mao, H. K.; Wu, Y.; Chen, L. C.; Shu, J. F.; Jephcoat, A. P. *J. Geophys. Res.* **1990**, *95*, 21–737.

Table 1. Crystal Structure Data for ε-Fe_3N_{1+x} for Refinements in Space Group *P*312 and $P6_322$

	space group, refined formula	
	*P*312, $Fe_3N_{1.08(2)}$	$P6_322$, $Fe_3N_{1.20(2)}$
a (Å)	4.7241(2)	
c (Å)	4.3862(2)	
V (Å^3)	84.773(6)	
Z	2	
D_{calcd} (g cm^{-3})	7.154	7.206
μ(Ag-K) (mm^{-1})	12.77	12.77
F(000) (e)	171.1	172.4
hkl range	−4 − 9, ±8, −8 − 7	
$2\theta_{max}$ (deg)	68.0	
no. of reflns measured	1088	
no. of unique reflns	477	244
R_{int}	0.0107	0.0127
Param. refined	21	14
R(F) $F_o > 4\sigma(F_o)$)	0.0189	0.0157
R(*F*)/*wR*(F^2) (all reflns)	0.0339/0.0556	0.0252/0.0377
GOF (F^2)	1.129	1.188
$\Delta\rho_{max}$ (e Å^{-3})	2.44	0.59

temperature, high-pressure treatment. It was earlier observed in a neutron powder diffraction study that ε-Fe_3N_{1+x} ($x = 0$, 0.10, 0.22) suffers increasing nitrogen disorder up to temperatures of about 700 K, while the samples started to decompose at temperatures above 750 K.[27,29] Considering the thermal instability of iron nitrides with respect to decomposition at such elevated temperatures, we interpret this crystallization of ε-Fe_3N under preservation of the nitrogen content as a diffusion-controlled process triggered by the high temperature, whereas the external pressure is necessary to prevent nitrogen loss.

From different high-pressure experiments, crystalline pieces of different sizes were selected for X-ray diffraction experiments. Larger crystals exhibit splitting of reflections at high diffraction angles because of pronounced mosaicity of the specimens. Therefore, we selected a very small crystal with distances of opposite faces below 20 μm. Table 1 gathers information concerning intensity collection and crystallographic properties. The crystal structure of ε-Fe_3N is based on the motif of a hexagonal close packing of iron with nitrogen in octahedral holes. In contrast to the binary iron nitrides γ′-Fe_4N and ζ-Fe_2N, the ε-phase exhibits an extremely broad homogeneity range in the sense of ε-$Fe_3N_{1\pm x}$. Figure 3 depicts the generally accepted phase diagram.[30,31] Ever since the pioneering work different space groups were discussed to describe the crystallographic ordering of nitrogen in ε-Fe_3N, respectively, within the homogeneity range of ε-$Fe_3N_{1\pm x}$.[32] Nitrogen atoms exhibit long-range occupational order in octahedral holes of the motif of a hexagonal close packing of iron leading to an crystallographic unit cell enlarged by $\sqrt{3} \times \sqrt{3} \times 1$ when compared to the simple *hcp* unit cell. As discussed earlier, the two most likely order mechanisms demand descriptions in the space groups $P6_322$ and *P*312, respectively.[27] Figure 4 visualizes the most important structural features, which will be discussed below.

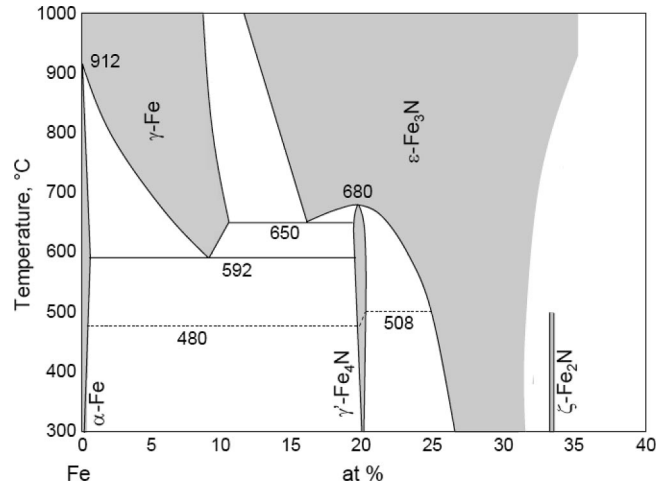

Figure 3. Phase diagram of the binary system Fe−N according to the literature.[30,31]

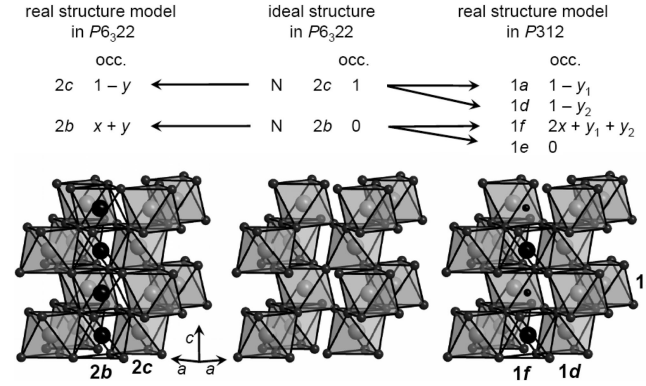

Figure 4. Comparison of the ideal structure for ε-Fe_3N (middle) in space group $P6_322$ and the models for the real structure of the ε-phase including nitrogen site disorder and deviation from the ideal composition. Left: Model in $P6_322$, additional occupation of site 2*b* indicated by black spheres in open octahedra. Right: Model in *P*312, site 2*c* is split in 1*a* and 1*d* with slightly different occupation deviating from unity and occupation of site 1*f* is visualized by black spheres in open polyhedra. Small black spheres indicate the unoccupied site 1*e*.

The ideal crystal structure of ε-Fe_3N ($Fe_3N_{1\pm x}$ with $x = 0$) with an ordered arrangement of nitrogen atoms is compatible with space group $P6_322$: All nitrogen atoms occupy Wyckoff position 2*c* leading to a three-dimensional framework of exclusively vertex-sharing octahedra $Fe_{6/2}N$. Additional octahedral voids within the hexagonal close packing of iron are located at the Wyckoff positions 2*b* and 2*d*; both are unoccupied in this idealized structural model. Occupation of the site 2*d* would connect the octahedra centered by nitrogen atoms at position 2*c* in direction [001] by sharing faces. Therefore, it is unlikely that these are occupied due to short interatomic distances and resulting pronounced Coulomb repulsions if nitrogen is viewed as negatively charged. This also holds for samples with larger nitrogen content or for a real-structure exhibiting partial disorder of nitrogen.

For an actual composition ε-Fe_3N_{1+x} we have to consider additionally occupied positions 2*b* within two likely models: In space group $P6_322$, an occupation of 2*b* sites leads to additional rods of face-sharing octahedra along [001], which are linked to the octahedra of the 2*c* position by common edges. Occupation is possible below a level of 50% in a

(29) Leineweber, A.; Jacobs, H.; Hüning, F.; Lueken, H.; Schilder, H.; Kockelmann, W. *J. Alloys Compd.* **1999**, *288*, 79.
(30) Jack, K. H. *Proc. R. Soc.London, A* **1951**, *208*, 200.
(31) Wriedt, H. A.; Gokcen, N. A.; Nafziger, R. H. *Bull. Alloy Phase Diagrams* **1987**, *8*, 355.
(32) Jack, K. H. *Acta Crystallogr.* **1952**, *5*, 404.

Table 2. Crystal Structure Parameters for ε-Fe_3N_{1+x} for Refinements in Space Group *P*312

atom	site	*x*	*y*	*z*	occ.	U_{eq} (Å^2)	U_{11}	U_{22}	U_{33}	U_{23}	U_{13}	U_{12}
Fe	6*l*	0.99689(6)	0.33197(7)	0.24995(5)	1	0.00670(8)	0.0070(1)	0.0063(1)	0.0061(1)	−0.00118(7)	−0.00042(9)	0.00280(8)
N(1)	1*a*	0	0	0	0.88(2)	0.0051(7)	0.005(1)	U_{11}	0.006(1)	0	0	1/2 U_{11}
N(2)	1*d*	$^1/_3$	$^2/_3$	$^1/_2$	0.82(2)	0.0060(9)	0.006(1)	U_{11}	0.006(2)	0	0	1/2 U_{11}
N(3)	1*f*	$^2/_3$	$^1/_3$	$^1/_2$	0.46(2)	0.009(2)	0.010(2)	U_{11}	0.009(4)	0	0	1/2 U_{11}

Table 3. Crystal Structure Parameters for ε-Fe_3N_{1+x} for Refinements in Space Group $P6_322$

atom	site	*x*	*y*	*z*	occ.	U_{eq}(Å^2)	U_{11}	U_{22}	U_{33}	U_{23}	U_{13}	U_{12}
Fe	6*g*	0.33051(6)	0	0	1	0.00671(8)	0.00737(9)	0.0063(1)	0.0061(1)	0.00133(7)	1/2 U_{23}	1/2 U_{22}
N(1)	2*c*	$^1/_3$	$^2/_3$	$^1/_4$	0.92(1)	0.0075(5)	0.0076(6)	U_{11}	0.0073(9)	0	0	1/2 U_{11}
N(2)	2*b*	0	0	$^1/_4$	0.28(1)	0.007(2)	0.008(2)	U_{11}	0.006(3)	0	0	1/2 U_{11}

disordered manner, thus limiting the number of face-sharing contacts. For small values of *x,* a random occupation of octahedra both within one row as well as in different parallel rows is feasible and therefore a description in space group $P6_322$ possible.

An ordered occupation of 50% crystallographic equivalent positions 2*b* in $P6_322$ in an alternating fashion along [001] would lead to a symmetry reduction to space group *P*312 if all parallel rods are in phase. This symmetry reduction to *P*312 is likely for large values of *x* in order to avoid face-sharing. However, the situation in ε-$Fe_3N_{1\pm x}$ is even more complex because each model of the real structure has to take into account a site occupation factor of site 2*c* below unity and a corresponding increased partial occupation of the additional octahedral voids.

Tables 1−3 give results of structure refinements performed on a good, but quite small crystal in both considered structure models. The refinement results for both space group choices indicate a real structure with about 10% vacancies at the nitrogen position of the idealized structure model of ε-Fe_3N, i.e., Wyckoff position 2*c* in $P6_322$ or positions 1*a* and 1*d* in *P*312, respectively.

An unambiguous discrimination of space group $P6_322$ and *P*312, respectively, can be realized by analyzing the reflection condition (00*l*) with $l = 2n + 1$. However, in case of ε-Fe_3N the reflections (00*l*) are only of the order $3\sigma(I)$. This observation is attributed to the overall low diffraction-intensity of the small crystal and the small value of *x* in combination with minute locally ordered domains. However, according to the Landau theory, a change in space group within a homogeneity range is not possible so that we can combine the findings of the present investigation with results of earlier studies and complementary data. Measurements of larger crystals that are not suitable for X-ray diffraction data collection always exhibit significant intensities for reflections (00*l*) for $l = 2n + 1$ with $n = 0, 1$. Additionally, an earlier study bears evidence for a weak reflection (001) in neutron powder diffraction data of a sample with composition $Fe_3N_{1.22}$.[27] Conversely, a close inspection of table 1 reveals slightly better quality criteria of the refinements for the structural model in space group $P6_322$. Reliability factors are lower due to better description of residuals in the final electron difference map. The largest peak in *P*312 corresponds to the position randomly occupied in $P6_322$, yet occupation converges to an occupation close to zero and to physically unreasonable displacement parameters in the refinements.

Table 4. Selected Bond Distances (Å) for ε-Fe_3N_{1+x} for Refinements in Space Group *P*312 and $P6_322$ with Estimated Standard Deviations in Parentheses

	*P*312	
Fe(1)	−N(1)	1.9195(3)
	−N(2)	1.9277(3)
	−N(3)	1.9096(3)
	$P6_322$	
Fe(1)	−N(1)	1.9244(1)
	−N(2)	1.9080(2)

Table 5. Total Energy Results for Fe_3N and $Fe_3N_{1.1}$

	Fe_3N	$Fe_3N_{1.1}$	
	*P*312/$P6_322$	*P*312	$P6_322$
Z	1	1	1
V (Å^3)	40.5	41.0	41.1
ΔH_f (kJ/mol)	−28.6	−22.6	−17.3
M (μ_B)	2.040	1.953	1.818
B_0 (GPa)	214	220	-

Table 6. Relative Energies upon Introducing Nitrogen Atoms into a Hexagonal-Close-Packed Structure of Iron in $P6_322$ (left) and *P*312 (right)

Wyckoff positions	ΔE (kJ/mol)	Wyckoff positions	ΔE (kJ/mol)
2*a*	301	1*e*+ 1*f*	99
2*b*	99	1*d*+ 1*f*	37
2*c*	0	1*a*+1*d*	0
2*d*	0		

As a summary, even local order compatible with the *P*312 symmetry causes reflections of the class (00*l*) with $l = 2n + 1$, which are forbidden in $P6_322$. For these, intensities are expected to be of the order of 0.05% of the strongest reflection of the $P6_322$ substructure for the given composition. Thus, the recent and earlier diffraction data consistently indicate a structural model with symmetry *P*312 rather than $P6_322$. Moreover, the refinement in *P*312 leads to a composition much closer to the expected composition (see above) than the alternative refinement in $P6_322$. In the preferred model, an alternating order of filled and empty additional octahedral voids is adopted locally. These polyhedra are interlinked to a 3D framework by vertex-sharing with the second type of octahedra having an occupation of the centers somewhat below unity. The refined distances Fe−N as given in Table 4 fall into the range of other iron nitrogen phases.

A theoretical analysis of the Fe_3N_{1+x} system (Table 5) led to the values presented in Table 6. For ε-Fe_3N, the space groups *P*312 and $P6_322$ generate identical structures.

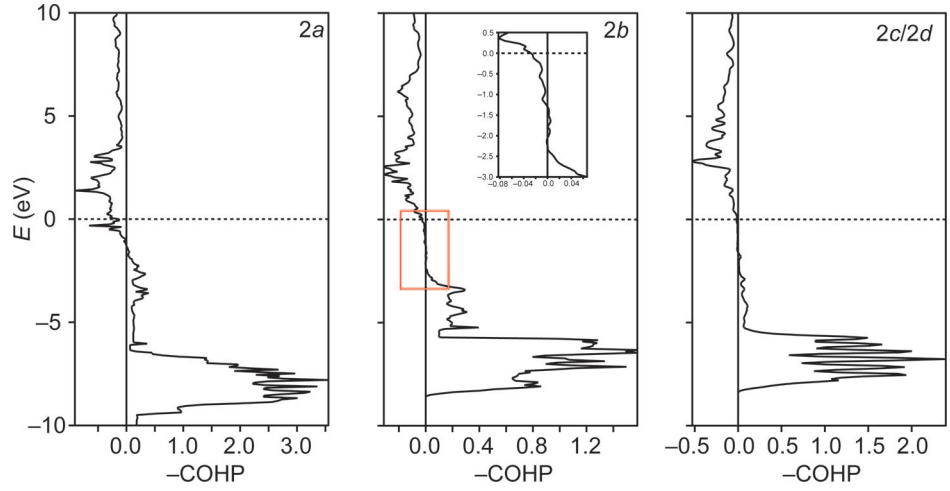

Figure 5. Comparison of the COHPs for nitrogen on different Wyckoff positions in ε-Fe_3N ($P6_322$).

In accordance to this, energy and volume are exactly the same. The enthalpy of formation ($\Delta H = -28.6$ kJ/mol) is more exothermic compared with the enthalpies of ζ-Fe_2N (−12.1 kJ/mol; exp, −3.8 kJ/mol[33]) and γ-Fe_4N (−20.4 kJ/mol; exp, −11.1 kJ/mol[33]). For the case of ε-$Fe_3N_{1.1}$, an analysis has to be performed showing which Wyckoff position will be occupied by the additional nitrogen atoms. Using a hexagonal-close-packed element iron in $P6_322$, there are four possible Wyckoff positions (2*a*, 2*b*, 2*c*, 2*d*). Table 6 shows that positions 2*c* and 2*d* are clearly favored. Position 2*b* is less suitable by 99 kJ/mol, whereas 2*a* is the worst candidate by 301 kJ/mol. The difference in energy can be explained with the COHPs (Figure 5) and the coordination of the nitrogen atoms by iron atoms. When position 2*a* is occupied, nitrogen is surrounded by three iron atoms lying in a plane. Because of this, the COHP diagram exhibits strong antibonding Fe−N interactions below the Fermi level. The nitrogen atoms on position 2*b* lie in an octahedral void, but these octahedra would be connected via face sharing, which is disfavored according to Pauling's rules and the resulting chain of octahedra is the reason for the small antibonding interaction just below the Fermi level. The positions lowest in energy are 2*c* and 2*d*. In both cases, the nitrogen atoms are located in octahedral voids, but this time the octahedra are connected via corners. Consequently, in the COHP diagram only bonding states can be seen below the Fermi level. According to Pauling's rules we find that the corner-shared octahedra (2*c*, 2*d*) are favored over the face-shared octahedra (2*b*). Just like in $P6_322$, the different Wyckoff positions were compared for *P*312. The positions 1*a* + 1*d* lie lowest in energy and are the same as 2*c* and 2*d* in $P6_322$, whereas 1*e* + 1*f* equal position 2*b*. The difference between *P*312 and $P6_322$ is that *P*312 offers another choice of N-atom distribution. When position 1*d* + 1*f* are occupied, the structure lies just 37 kJ/mol higher in energy than the lowest combination 1*a* + 1*d*. This means that, if nitrogen occupies more than one position, the above space groups can be distinguished. To do so, different supercells

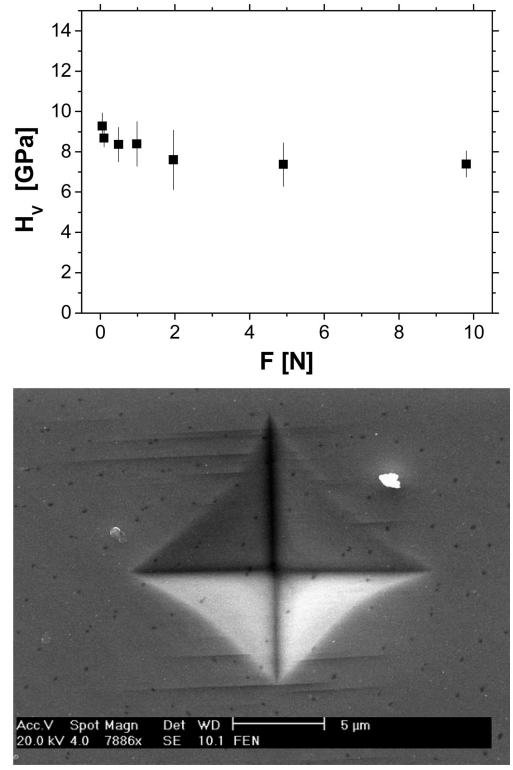

Figure 6. Top: Vickers microhardness of ε-Fe_3N_{1+x} crystals as a function of applied load. Bottom: SEM micrograph of the Vickers indentation obtained with load of 0.98 N.

with the composition $Fe_3N_{1.1}$ were built according to the site preferences of nitrogen occupation found in the prior calculations for the ideal composition Fe_3N_1. We found that *P*312 is favored over $P6_322$ in $Fe_3N_{1.1}$ by 5 kJ/mol. The formation of ε-$Fe_3N_{1.1}$ is an exothermic process (−22.6 kJ/mol) and the calculated bulk modulus (220 GPa) is in satisfying agreement with the experimental one. There is a small lowering of the magnetic properties, when N atoms are introduced into ε-Fe_3N (2.04 μ_B) to give ε-$Fe_3N_{1.1}$ (1.95 μ_B).

The results of the Vickers hardness measurement are presented in Figure 6. The average H_V from six indentations at 0.5 kg and two indentations at 1 kg is analyzed to be 7.4(10) GPa. Typical load-displacement curves obtained by

(33) Blachnik, R.; *D'Ans & Lax: Taschenbuch für Chemiker und Physiker, Teil 3*; Springer: Berlin, 1998.

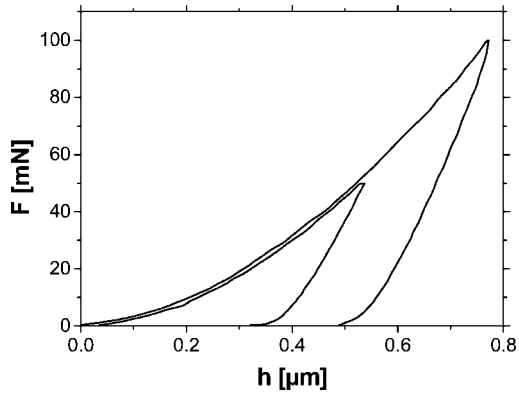

Figure 7. Typical load-displacement curves, $F(h)$, for ε-Fe_3N_{1+x} measured by nanoindentation technique.

the nanoindentation experiment are shown in Figure 7. The average values for the nanoindentation hardness H and for the reduced elastic modulus E_r of ε-Fe_3N_{1+x} were determined to be 10.1(8) GPa and 178(11) GPa, respectively. The hardness of the synthesized ε-Fe_3N_{1+x} crystals is significantly higher than that of pure iron ($\sim$0.3 − 2 GPa) and is in the range of tool steels (up to 9 GPa) and nitrided steels ($\sim$5 − 15 GPa).[34−37] Comparably high standard deviations of the measured hardness and of the reduced elastic modulus of ε-Fe_3N_{1+x} are most probably due to anisotropy of the investigated material. In particular, E_r was found to vary from about 165 to 196 GPa depending on the indented crystallite. However, the orientation of the indented crystallites was not determined in the present work.

Finally, we estimated the shear modulus (G_0), the Young's modulus (E_0), and the Poisson's ratio (υ_0) of polycrystalline ε-Fe_3N_{1+x} using experimental values for B_0 and E_r. For this purpose, the well-known relations between isotropic E, B, G, and υ, namely $E = 9BG/(3B + G)$ and $\nu = (1/2)(3B - 2G)/(3B + G)$,[38] were substituted in the equation defining E_r: $1/E_r = (1 - \nu_0^2)/E_0 + (1 - \nu_i^2)/E_i$, where $E_i = 1141$ GPa is the Young's modulus and $\upsilon_i = 0.07$ the Poisson's ratio of the indenter material, namely diamond.[20] Here we assumed that the average reduced elastic modulus of ε-Fe_3N_{1+x} measured by nanoindentation is that of isotropic polycrystalline material. Applying $B_0 = 172(4)$ GPa and $E_r = 178(11)$ GPa in the above-mentioned equations we derived $G_0 = 78(8)$ GPa as the shear modulus, $E_0 = 203(22)$ GPa as the Young's modulus and $\upsilon_0 = 0.32(4)$ as the Poisson's ratio for polycrystalline ε-Fe_3N_{1+x}. This experimental Young's modulus results about 20% lower than derived from quantum mechanical calculations (243 GPA), the Poisson's ratio is identical within the estimated error (0.29).[39]

Conclusions

We have studied the high-pressure behavior of the binary iron nitride ε-Fe_3N_{1+x}, which is long known as a traditional hard material. *In-situ* X-ray diffraction experiments revealed a bulk modulus of $B_0 = 172(4)$ GPa ($B' = 5.7$, fixed). We find a calculated bulk module (220 GPa) which is in good agreement with the experimental one. Ex situ high-temperature-high pressure experiments produced reproducibly bulk single crystalline material ε-Fe_3N_{1+x} in a pressure-induced crystal growth. Micro- and nanoindentation measurements revealed a material, significantly harder than pure iron, with a hardness in the range reported for nitrided steels. The preferred structural model in space group $P312$ is suggested because of observation of small diffraction intensities of reflections forbidden in $P6_322$ and considerations concerning an energetically favorable nitrogen atom order. In accordance with the experimental findings, electronic structure calculations reveal a slightly higher stability (5 kJ/mol) for $P312$, which can be explained by a Fe−N bonding analysis and the favorable coordination environment of the nitrogen atoms.

Acknowledgment. We thank Anja Völzke for performing the chemical analyses, Susann Müller for the operating of the thermal analysis, and Claudia Wasmund for assistance in the nanoindentation experiments. Additionally, we acknowledge the assignment of beamtime at the undulator beamline ID 9A of the ESRF. We also thank the computer centre of the RWTH Aachen and the Jülich supercomputing centre for providing computer resources. This work was supported by the Elitenetzwerk Bayern within the Advanced Materials Science program, the Max-Planck-Gesellschaft, and within the priority program "Synthesis, in situ characterisation and quantum mechanical modelling of Earth Materials, oxides, carbides and nitrides at extremely high pressures and temperatures" of the Deutsche Forschungsgemeinschaft (SPP 1236). R.R. acknowledges the financial support by the Fonds der Chemischen Industrie, Frankfurt, Germany.

Supporting Information Available: CIF files for the structure refinements in space groups $P312$ and $P6_322$. This materials is available free of charge via the Internet at http://pubs.acs.org.

CM802721K

(34) Brandes, E. A.; Brook, G. B. *Smithells Metals Reference Book*, 7th ed.; Butterworth-Heinemann: Oxford, U.K., 1997.
(35) Oberg, E.; Jones, F. D.; Horton, H. L.; Ryffel, H. H. *Machinery's Handbook*, 27th ed.; Industrial Press: New York, 2004.
(36) Weber, T.; de Wit, L.; Saris, F. W.; Königer, A.; Rauschenbach, B.; Wolff, G. K.; Krauss, S. *Mater. Sci. Eng.* **1995**, *A199*, 205.
(37) Guemmaz, M.; Moser, A.; Grob, J.-J.; Stuck, R. *Surf. Coat. Technol.* **1998**, *100*, 353.
(38) Landau, L. D.; Lifshitz, E. M. *Theory of Elasticity*, 2nd ed.; Pergamon Press: London, 1975.
(39) Gressmann, T.; Leineweber, A.; Mittermeijer, E. J. *Philos. Mag.* **2008**, *88*, 145.